

Key factors affecting graphene oxide transport in saturated porous media

Original

Key factors affecting graphene oxide transport in saturated porous media / Beryani, Ali; Alavi Moghaddam, M. R.; Tosco, T.; Bianco, C.; Hosseini, S. M.; Kowsari, E.; Sethi, R.. - In: SCIENCE OF THE TOTAL ENVIRONMENT. - ISSN 0048-9697. - 698:(2020), p. 134224. [10.1016/j.scitotenv.2019.134224]

Availability:

This version is available at: 11583/2784318 since: 2020-01-23T10:24:42Z

Publisher:

Elsevier B.V.

Published

DOI:10.1016/j.scitotenv.2019.134224

Terms of use:

This article is made available under terms and conditions as specified in the corresponding bibliographic description in the repository

Publisher copyright

(Article begins on next page)

Key factors affecting graphene oxide transport in saturated porous media

Ali Beryani^{(1)(a)}, Mohammad Reza Alavi Moghaddam^{(1)(*)}, Tiziana Tosco⁽²⁾, Carlo Bianco⁽²⁾, Seiyed Mossa Hosseini⁽³⁾, Elaheh Kowsari⁽¹⁾, Rajandrea Sethi⁽²⁾

(1) Department of Civil and Environmental Engineering (CEE), Amirkabir University of Technology, Hafez Ave., 424, 15875-4413, Tehran, Iran

(2) Department of Environmental, Land and Infrastructure Engineering, Politecnico di Torino, Corso Duca degli Abruzzi 24 10129, Torino, Italy

(3) Physical Geography Department, University of Tehran, 16th Azar St., Enghelab Sq., 14155-6465, Tehran, Iran.

(a) Present address: Department of Environmental, Land and Infrastructure Engineering, Politecnico di Torino, Corso Duca degli Abruzzi 24 10129, Torino, Italy

(*) Corresponding author: alavi@aut.ac.ir, alavim@yahoo.com, tel. +98 021 64543008

Revised manuscript submitted to

Science of the Total Environment

July 2019

26

Abstract

27

This study focuses on the transport in porous media of graphene oxide nanoparticles (GONP) under conditions similar to those applied in the generation of *in-situ* reactive zones for groundwater remediation (i.e. GO concentration of few tens of mg/l, stable suspension in alkaline solution). The experimental tests evaluated the influence on GO transport of three key factors, namely particle size (300–1200 nm), concentration (10–50 mg/L), and sand size (coarse to fine). Three sources of GONP were considered (two commercial and one synthesized in the laboratory). Particles were stably dispersed in water at pH 8.5 and showed a good mobility in the porous medium under all experimental conditions: after injection of 5 pore volumes and flushing, the highest recovery was around 90%, the lowest around 30% (only for largest particles in fine sand). The particle size was by far the most impacting parameter, with increasing mobility with decreasing size, even if sand size and particle concentration were also relevant. The source of GONP showed a minor impact on the mobility. The transport test data were successfully modeled using the advection-dispersion-deposition equations typically applied for spherical colloids. Experimental and modeling results suggested that GONP, under the explored conditions, are retained due to both blocking and straining, the latter being relevant only for large particles and/or fine sand. The findings of this study play a key role in the development of an in-situ groundwater remediation technology based on the injection of GONP for contaminant degradation or sorption. Despite their peculiar shape, GONP behavior in porous media is comparable with spherical colloids, which have been more studied by far. In particular, the possibility of modeling GONP transport using existing models ensures that they can be applied also for the design of field-scale injections of GONP, similarly to other particles already used in nanoremediation.

49

50

51

Keywords:

52

Graphene oxide, transport in porous media, nanoparticle size effect, blocking, straining, nanoremediation

53

54

55

Highlights:

56

Graphene oxide transport is controlled by blocking and straining phenomena

57

Graphene oxide mobility in porous media strongly depends on its lateral size

58

A power law correlates the attachment/detachment coefficients to GO particle size

59

Good mobility/stability of GO makes it potentially capable in groundwater remediation

60

61

62

1. Introduction

Graphene oxide nanoparticles (GONP) are carbon-based irregular 2D flakes with a nanoscale thickness (Chen et al., 2012). GONP contain large amounts of oxygenated functional groups at the surface, such as carbonyl, carboxyl, hydroxyl, and phenol (Huang et al., 2011). They have been studied for several, diverse applications, e.g. in electronics, biomedicine, and sensors (Liu et al., 2013a; Novoselov et al., 2012; Qi et al., 2014a; Tortello et al., 2016). More recently, laboratory studies showed that GO can effectively remove several organic contaminants (Akpotu and Moodley, 2018; Iqbal and Abdala, 2013; Yang et al., 2013) and heavy metals (Jiang et al., 2018; Yin et al., 2019; Zhao et al., 2019; Zhou et al., 2016) from contaminated water. This evidence opens perspectives for several environmental applications, including wastewater treatment and in-situ remediation of contaminated aquifer systems, in particular for the removal of recalcitrant compounds and specific contaminants of concerns.

For the in-situ remediation the reference technology is the nanoremediation, that is, the injection of nanoparticles into the contaminated aquifer system for degradation, sorption precipitation or complexation of organic or inorganic contaminants (Corsi et al., 2018; Karn et al., 2009; O'Carroll et al., 2013; Patil et al., 2016; Tosco et al., 2014). The reactive particles must be dispersed and stably suspended in water-based slurries, thus allowing effective injection and targeting of the treatment area, which can be accomplished only with a strong control of the particle mobility in the porous medium. As a consequence, it is of pivotal importance to understand the main operative parameters controlling particle transport in the porous medium, and to develop reliable transport models to predict the particle mobility during injection and the final distribution of the reactive material. In this work, we study at a laboratory scale the potential injectability of GONP in the subsurface, which is a crucial aspect for the use of any nanoparticle for in situ treatment of a contaminated aquifer. In particular,

87 we study how GONP transport in porous media is affected by those parameters which usually
88 play a key role in nanoparticle injection for groundwater remediation, namely particle size
89 and concentration, and porous medium size.

90 Compared to other materials already used for nanoremediation, eg. zero valent iron NPs,
91 GONP inherently possess negative charges under a wide range of different environmental
92 conditions, and can be easily dispersed in aqueous solutions, remaining suspended for a long
93 period, even in the absence of stabilizers (Liu et al., 2013b; Qi et al., 2014a). Moreover, up to
94 now most studies demonstrated that GONP tend to poorly interact with the porous medium,
95 and therefore are retained on sand grains in limited amounts (Dong et al., 2016; Fan et al.,
96 2015a; Feriencikova and Xu, 2012; Lanphere et al., 2013; Liu et al., 2013a; Liu et al., 2013c;
97 Qi et al., 2014a; Sun et al., 2015; Xia et al., 2019). Thus, previous studies suggest a good
98 potential mobility of GONP in aquifers and a relatively easy injectability at the field scale,
99 compared to other nanoparticles already employed in the nanoremediation.

100 Until now, studies have been published on the suspension stability, transport and retention of
101 GONP in porous media (Lanphere et al., 2014; Li et al., 2016; Liu et al., 2013b; Wang et al.,
102 2017). However, they mostly focused on the influence of solution chemical parameters such
103 as pH, ionic strength (IS), ion valence, and natural organic matter (NOM) concentration,
104 which all play a key role on the long term fate of GONP in aquifer systems (Chrysikopoulos
105 et al., 2017; Fan et al., 2015a; Fan et al., 2015b; Feriencikova and Xu, 2012; Jian-Zhou et al.,
106 2015; Lanphere et al., 2013; Liu et al., 2013b; Liu et al., 2013c; Lu et al., 2017; Peng et al.,
107 2017; Qi et al., 2014a; Xia et al., 2019). In particular, the influence of ion concentration and
108 valence is now relatively well understood. Conversely, in this work we focus mainly on
109 particle size and concentration and their physical interactions with porous media of different
110 grain size; all these parameters become extremely relevant when particle suspensions are
111 injected on purpose in the subsoil.

112 Particle size is known to play a critical role in colloid transport, as already elucidated by a
113 broad literature, from colloid filtration theory and beyond. The porous medium grain size can
114 have a huge impact on the colloid transport and retention, as predictable by the colloidal
115 filtration theory (CFT) (Tufenkji and Elimelech, 2004; Yao et al., 1971). However, a direct
116 extension of known processes and modeling approaches to GONP is not necessarily
117 straightforward, due to the peculiar shape of such platelets. To the authors' knowledge, no
118 previous study has already investigated and quantified the influence of particle size on GONP
119 transport, and a few studies (Dong et al., 2019; Sun et al., 2012) have investigated the grain
120 size effect on the transport and retention of GONP. Also, there is a lack of systematic
121 information about the relationship between size of plate-like nanoparticles and their retention
122 kinetic parameters. In this study, we consequently develop empirical equations expressing
123 this relationship.

124 As a general rule, when colloidal suspensions are fairly stable and particles are sufficiently
125 small compared to pore size to avoid straining and filtration phenomena, the injected
126 concentration has a limited impact on particle transport, which is dominated by blocking
127 phenomena (Tosco et al., 2014). This is the case of colloidal suspensions like bacteria,
128 carboxylic latex, silica, titania and silver nanoparticles, and carbon nanotubes (Bradford and
129 Bettahar, 2006; Bradford et al., 2009; Camesano and Logan, 1998; Godinez and Darnault,
130 2011; Kasel et al., 2012; Liang et al., 2013; Wang et al., 2012; Zhang et al., 2010). When
131 considering the injection of particle suspensions for nanoremediation, graphene oxide is
132 expected to be injected in relatively high concentrations (eg. several tens of mg/L) and then
133 diluted in groundwater. In these conditions, the injected concentration often plays a major role
134 in particle mobility and distribution in the porous medium. Sun et al. (2015) found that GONP
135 mobility into sand-packed columns increased at higher input concentrations, coherently with
136 the good colloidal stability of graphene oxide suspensions. In the present work, the impact of

137 the injected concentration on GONP mobility is further studied, extending the range of
138 conditions explored in the cited study.

139 In light of what discussed above, the aim of the present research is to elucidate unexplored or
140 still unclear aspects related to GONP transport in porous media under conditions which could
141 be expected for its application in nanoremediation, and to provide a reliable modeling
142 framework able to correctly reproduce the observed processes. Column transport tests were
143 performed using different graphene oxide types, particle size, injected concentration and sand
144 samples. The experimental results were modeled using a well-established advection-
145 dispersion-deposition equation for particle transport, using the numerical solution provided
146 by the software MNMs (Bianco et al., 2016). Afterwards, the dependence of the model
147 coefficients on the abovementioned parameters was quantified.

148

2. Materials and methods

2.1. GONP suspensions

In this study, three types of graphene oxide were used, identified as GO₁, GO₂, and GO₃ (Table 1). GO₁ (Graphenea Inc., Spain) is a single-layer graphene oxide dispersion, provided in a concentrated stock solution (4 g/L). GO₂ (Cheap Tubes Inc., US) is a single-layer GO provided in a dry powder ;from ,a stock solution (2 g/L) was then prepared by suspending the particles in DI water. GO₃ was synthesized in the laboratory following an eco-friendly improved Hummer's method developed by Chen et al. (2013), and stored in a stock solution at 1.45 g/L.

The synthesized GO₃ was characterized into details using the following methods: energy-dispersive X-ray spectroscopy (EDX, Octane SDD equipped with the SUTW detector, EDAX, United States), Fourier transform infrared spectroscopy (FT-IR, Bruker FTIR Equinox 55 spectroscopy, equipped with a MCT cryo-detector, Germany), X-ray diffraction (XRD, Equinox 3000, Inel, United States), Atomic Force Microscopy (AFM, NTEGRA AFMNT-MDT, NT-MDT Spectrum Instruments, Russia), and Field Emission Scanning Electron Microscopy (FE-SEM, Supra 40, ZEISS, Germany). The results of the characterization are reported in the Supporting Information. For the commercial GO₁ and GO₂ samples similar analyses were provided by the manufacturers (see SI for references).

Table 1: Characteristics of GO₁, GO₂, and GO₃

Name	Producer	Synthesis method	Size range after sonication (μm) (*)	Number of layers (**)	Thickness of layers (nm) (**)	Elemental analysis (***)			
						Carbon % (w/w)	Oxygen % (w/w)	Hydrogen % (w/w)	Sulfur % (w/w)
GO ₁	Graphenea	Modified Hummer's method	0.3-1.6	1	0.8~1.2	49-56	41-50	0-1	2-4
GO ₂	Cheap Tubes	Modified Hummer's method	0.3-0.8	1	0.7~1.2	35-42	45-55	3-5	-
GO ₃	Own synthesis	Improved Hummer's method (without using NaNO ₃)	0.9-1.5	1-2	0.8~2	45-60	40-55	-	<1

(*) DLS measurements
(**) AFM analysis for GO₃, manufacturers' data sheets for GO₁ and GO₂
(***) EDX analysis for GO₃, manufacturers' data sheets for GO₁ and GO₂

168

169 Size and zeta potential measurements were performed using dynamic light scattering (DLS)
170 (Zetasizer Nano ZSP, Malvern Instruments, UK) for the three GO types.

171 For all tests, the GONP suspension was prepared immediately before injection by: diluting
172 the stock solution to the desired GO concentration with DI water, applying probe sonication
173 (UP200s Hielscher Ultrasound Technology, Germany), adding NaCl and NaOH to adjust,
174 respectively, ionic strength (20 mM) and pH (8.5±0.5), and degassing in a vacuum chamber
175 to remove residual air micro-bubbles. For GO₁ and GO₃, a different sonicating duration was
176 used to adjust the average size of the particles (see detailed discussion on paragraph 3.1) and
177 for GO₂ a 5 mins sonication was performed. The pH value was selected as typical value for
178 GONP suspensions with good colloidal stability, which is therefore expected to be used in
179 case of GO application to groundwater nanoremediation.

180

2.2. Porous medium

181 Silica sand with a minor content of K-feldspar (Sibelco, Dorfner, Germany) was sieved to
182 obtain three different size ranges: coarse S₁ (0.3~1.0 mm, d₅₀=0.75 mm), medium S₂ (0.25~0.5
183 mm, d₅₀=0.4 mm), and fine S₃ (0.075~0.6 mm, d₅₀=0.28 mm). Prior to column packing, to

184 remove fine suspended solids, metal oxides and other possible impurities, the sand was
185 cleaned following the procedure reported in (Liu et al., 2013b; Qi et al., 2014a; Sun et al.,
186 2015; Tosco et al., 2009). The zeta potential of the sand was measured (Zetasizer Nano ZSP,
187 Malvern) following the method developed by Johnson et al. (1996). The measured values of
188 zeta potential were -38 ± 2 , -40 ± 1 and -42 ± 2 mV for S_1 , S_2 , and S_3 in 20 mM NaCl solution at
189 pH 8.5, respectively.

191 **2.3. GONP transport tests**

192 A Plexiglas cylinder (length 15.2 cm, inner diameter 1.6 cm) was wet-packed with degassed
193 sand following the protocol detailed by Tosco et al. (2012). The column experiments were
194 performed at a constant injection rate of 1.63×10^{-8} m³/s, resulting in a Darcy velocity of
195 8.11×10^{-5} m/s. GONP suspensions were prepared following the protocol described in
196 paragraph 2.1 at concentrations of 50, 20, 15 and 10 mg/L, representative of GONP
197 concentrations applicable for field injections. The injection protocol involved the following
198 steps:

- 199 - Pre-equilibration of the column with DI water for 5 pore volumes (PVs);
- 200 - Pre-flushing with background electrolyte solution (NaCl 20 mM) for 5 PVs;
- 201 - Injection of the GONP suspension in the background electrolyte solution for 4.5 PVs;
- 202 - Flushing with the background electrolyte solution for 4 PVs;
- 203 - Final flushing with DI water for 5 PVs (only for selected column tests).

204 During the experiments, salt and GONP concentrations were continuously measured at the
205 column inlet and outlet using an UV-Vis Spectrophotometer (Specord S600, Analytik Jena,
206 Germany) equipped with flow-through quartz cells with 5 mm light path (Hellma, Germany).
207 The concentration was continuously monitored at a measurement frequency of 10 seconds at
208 wavelengths of 198 nm (for dissolved species) and 230 nm (for GONP).

For each column test, the effective porosity (ϵ) and the dispersivity (α) were determined via inverse fitting of the NaCl breakthrough curve (BTC), according to (Bianco et al., 2016). An average effective porosity of 0.49(\pm 0.015), 0.47(\pm 0.005), and 0.44(\pm 0.015) and an average dispersivity of 5.16(\pm 0.784) $\times 10^{-4}$ m, 4.87(\pm 0.589) $\times 10^{-4}$ m, and 3.97(\pm 0.813) $\times 10^{-4}$ m were obtained for the sands S₁, S₂, and S₃, respectively. The detailed results for each column test are reported in Table S1.

At the end of each column test, the sand column was dissected into five sections of 3 cm each to determine the profiles of retained GO mass and average particle size. The dissection procedure and the validation of concentration profiles against breakthrough curve mass balances are detailed in SI.

The GONP column transport tests were performed using different combinations of GO type (GO₁, GO₂, and GO₃), size and concentration, as well as different sand average size to systematically investigate the influence of these parameters on the transport of GONP.

2.4. GONP transport and retention modeling

The transport and retention of GONP in 1D saturated porous media was modeled using the general formulation of the advection-dispersion equation modified to include the particle mass exchange (deposition and release) between liquid and solid phase (Bradford and Bettahar, 2006; Bradford et al., 2003; Hosseini and Tosco, 2013; Qi et al., 2014a; Qi et al., 2014b; Tosco and Sethi, 2010; Wang et al., 2011) implemented in MNMs (<https://areeweb.polito.it/ricerca/groundwater/software>):

$$\begin{cases} \frac{\partial}{\partial t}(\epsilon C) + \sum_i \left(\rho_b \frac{\partial S_i}{\partial t} \right) = - \frac{\partial}{\partial x}(qC) + \frac{\partial}{\partial x} \left(\epsilon D \frac{\partial C}{\partial x} \right) \\ \rho_b \frac{\partial S_i}{\partial t} = f_i(C, S_i) = \epsilon k_{a,i} \psi_i C - \rho_b k_{d,i} S_i \end{cases} \quad (\text{eq. 3})$$

231 where C is the concentration of the nanoparticles in the liquid phase [$M L^{-3}$], t is time [T], ϵ
 232 is the medium porosity [-], i is a subscript regarding to the i^{th} interaction site, ρ_b is the bulk
 233 density of the porous medium [$M L^{-3}$], S_i is the mass concentration of nanoparticles deposited
 234 on the i^{th} site [$M M^{-1}$], x is the distance traveled from the inlet [L], q is Darcy flow rate [$L T^{-1}$],
 235 D is the dispersion coefficient [$L^2 T^{-1}$], $k_{a,i}$ and $k_{d,i}$ are the attachment and detachment
 236 kinetic coefficients, respectively [T^{-1}], and ψ_i is a function controlling the interaction
 237 dynamics of colloid deposition for i^{th} site.

238 In this study, a 2-site model considering two interaction mechanisms was used to describe
 239 particle interactions with the porous medium, namely, a physico-chemical
 240 attachment/detachment site with a maximum retainable concentration $S_{\max,1}$ [$M M^{-1}$]
 241 (reversible blocking site, $i=1$) and a second site describing the physical retention of the
 242 nanoparticles (irreversible straining site, $i=2$). For the second interaction mechanism, the
 243 formulation proposed by Bradford et al. (2004; 2003) was adopted:

$$244 \quad \psi_1 = \left(1 - \frac{S_1}{S_{\max,1}}\right) \quad (\text{eq.2})$$

$$245 \quad \psi_2 = \left(1 + \frac{x}{d_{50}}\right)^{\beta_{str,2}} \quad (\text{eq.3})$$

246 where d_{50} is the mean size of sand grains [L], and $\beta_{str,2}$ [-] is a kinetic exponent controlling the
 247 shape of the spatial distribution of retained nanoparticles.

248 The experimental breakthrough curves (BTCs) of GONP were fitted to the mathematical
 249 model using MNMs. The fitting parameters include the attachment/detachment kinetics ($k_{a,1}$,
 250 $k_{d,1}$, $k_{a,2}$) and the maximum retainable concentration $S_{\max,1}$. The exponent $\beta_{str,2}$ was assumed
 251 equal to the value proposed in the literature (0.432) with good results (Bradford et al., 2003).

252 **3. Results and discussions**

253 **3.1. Characterization of synthesized GONP (GO₃)**

254 EDX analysis indicated that GO₁ and GO₃ contain similar percentages of C and O (Table 1).
255 For GO₂ the produce reports a slightly higher content of C and lower of O. FT-IR transmission
256 spectra confirmed for GO₃ the existence of epoxide (–O–), carbonyl (–C=O), carboxyl (–
257 COOH) and hydroxyl (–OH) functional groups on the GO₃ surface (Figure S2). The XRD
258 pattern of dried GO₃ showed a reflection peak at $2\theta=12^\circ$, corresponding to d-space of 0.741
259 nm (Figure S3). This large interlayer spacing between the sheets implies the existence of
260 oxygenated functional groups produced by the harsh chemical oxidation of pure graphite
261 (with the smaller initial d-spacing of about 0.3 nm) and the formation of graphene oxide (Chen
262 et al., 2013; Paulchamy et al., 2015; Shahriary and Athawale, 2014).

263 The specific surface area of the GO₃ (989 m²/g) was estimated using the methylene blue
264 titration method proposed by Montes-Navajas et al. (2013). The experimental procedure and
265 calculations of specific surface area are detailed in the SI (Figure S4).

266 AFM analysis indicated that the synthesized GO₃ suspension (in DI, after 45 seconds ultra-
267 sonication) consisted of single- or two-layer flakes with thickness 0.8~2 nm (Figure S5) and
268 lateral size of 500~1000 nm. AFM analysis of GO₂ provided by the manufacturer evidenced
269 a similar thickness (up to 3 nm). FE-SEM analysis also showed that the lateral size of GO₃
270 after synthesis (without size adjustment) ranged between 900~1500 nm (Figure S6).

271 GONP formed stable colloidal suspensions: kinetic aggregation measurements using DLS
272 (Figure S7) and visual sedimentation tests (not reported) indicated that the three GONP were
273 all stably dispersed in a 20 mM NaCl solution for at least two hours (i.e. longer than the
274 duration of the transport tests). This is in agreement with the strongly negative values of Zeta
275 potential measured for the suspensions (-50 ± 4 , -55 ± 6 , and -56 ± 1 mV for GO₁, GO₂, and GO₃,
276 respectively).

277 It was observed that applying probe sonication for a different duration the average size of the
278 GONP in suspension changes: the longer the duration, the smaller the average size (Figure

279 S8). Particle size distribution is broader if no sonication is applied, or applied for short
280 durations, and becomes narrower when sonication is prolonged (3 mins or higher). Sonication
281 did not significantly alter other properties of the GONP (colloidal stability and zeta potential,
282 compare Figure S9). Consequently, based on these results, the average size of GO₁ and GO₃
283 (Table 2) was controlled by changing the duration of probe sonication during the suspension
284 preparation, following Figure S8.

285 It is worth to mention that, due to their platelet-like shape, GONP size measurements obtained
286 from DLS cannot be directly interpreted as the correct size of the particles, and are rather
287 related to both platelet lateral size, shape and thickness, as discussed in the literature (Lotya
288 et al., 2013). Consequently, in this work the measured average size values were used as a
289 semi-quantitative measurement of the lateral size, and changes in average size were analyzed
290 mainly in terms of particle size increase/decrease, rather than absolute values. The actual
291 lateral size was instead obtained from SEM and AFM measurements (see Supporting
292 Information).

293 **3.2. Column transport tests**

294 The GONP column transport tests were performed using different combinations of GO type
295 (GO₁, GO₂, and GO₃), lateral size and concentration, as well as different sand average size to
296 systematically investigate the influence of these parameters on the transport of graphene oxide
297 (Table 2). The observed and simulated BTCs were normalized to the injected concentration
298 (C/C_0) and reported as a function of pore volumes (Figure 1, Figure 4, and Figure 6). In the
299 graphs, P.V. = 0 (time $t = 0$) corresponds to the beginning of GO injection, thus equilibration
300 and pre-flushing steps are not reported. The retention profiles were reported as a normalized
301 concentration of deposited GONP (S , namely mass of GONP normalized to the sand mass)
302 (Figure 2, Figure 5, and Figure 7).

303 The experimental BTCs were fitted using the 2-site retention model equations (1-3). As a
304 general rule, the results indicated that under the tested experimental conditions the model
305 equations can satisfactorily simulate the observed BTCs of GONP (for all the experiments
306 $R^2 > 0.99$) with a very little mismatch in both rising and tailing parts of the BTCs. For GO_2
307 only, in some cases, the second site (straining) had a negligible effect on the particle transport
308 and was therefore removed. The fitted model parameters are summarized in Table 2.

309 The low values of $k_{d,1}$ (detachment coefficient for blocking deposition) obtained for all the
310 tests indicated that physico-chemical deposition will be practically irreversible if the ionic
311 strength (and therefore the particle-collector electrostatic interactions) is not modified. This
312 is coherent with the negligible tailing observed in the experimental breakthrough curves. A
313 few additional tests were performed flushing the columns after particle deposition with
314 stepwise decreasing salt concentration. The results (Figure S10) revealed that particles
315 retained due to physical-chemical interactions are not readily mobilized unless a strong
316 decrease in salt concentration is applied (in our experiments, NaCl concentration below 5
317 mM).

321

Table 2: Experimental conditions of column transport tests and fitted coefficients ($k_{a,1}$, $k_{d,1}$,

322

 $S_{max,1}$, and $k_{a,2}$)

Test No.	GO Type	C_0 (mg/L)	GO Size (nm)	Sand	$k_{a,1}$ [s^{-1}]	$k_{d,1}$ [s^{-1}]	$S_{max,1}$ [g/g]	$k_{a,2}$ [s^{-1}]
1	GO ₁	50	898±47	Coarse	$6.06 \cdot 10^{-4}$	$8.34 \cdot 10^{-5}$	$5.38 \cdot 10^{-6}$	$4.70 \cdot 10^{-4}$
2		50	1000±49	Medium	$1.20 \cdot 10^{-3}$	$8.18 \cdot 10^{-6}$	$4.79 \cdot 10^{-6}$	$1.90 \cdot 10^{-3}$
3		50	984±55	Fine	$2.30 \cdot 10^{-3}$	$3.54 \cdot 10^{-5}$	$9.00 \cdot 10^{-6}$	$3.10 \cdot 10^{-3}$
4		20	1128±111	Coarse	$9.07 \cdot 10^{-4}$	$5.00 \cdot 10^{-5}$	$3.25 \cdot 10^{-6}$	$1.40 \cdot 10^{-3}$
5		20	1100±63	Medium	$2.50 \cdot 10^{-3}$	$3.20 \cdot 10^{-5}$	$5.36 \cdot 10^{-6}$	$2.40 \cdot 10^{-3}$
6		20	1076±59	Fine	$2.44 \cdot 10^{-3}$	$2.92 \cdot 10^{-5}$	$4.90 \cdot 10^{-6}$	$5.28 \cdot 10^{-3}$
7		15	1122±72	Fine	$2.90 \cdot 10^{-3}$	$1.81 \cdot 10^{-5}$	$4.93 \cdot 10^{-6}$	$6.20 \cdot 10^{-3}$
8		10	1082±69	Fine	$3.60 \cdot 10^{-3}$	$5.47 \cdot 10^{-5}$	$3.46 \cdot 10^{-6}$	$8.90 \cdot 10^{-3}$
9		20	1286±332	Fine	$4.08 \cdot 10^{-3}$	$2.34 \cdot 10^{-5}$	$4.72 \cdot 10^{-6}$	$9.30 \cdot 10^{-3}$
10		20	980±40	Fine	$2.51 \cdot 10^{-3}$	$3.46 \cdot 10^{-5}$	$5.44 \cdot 10^{-6}$	$5.70 \cdot 10^{-3}$
11		20	820±70	Fine	$1.88 \cdot 10^{-3}$	$3.49 \cdot 10^{-5}$	$4.87 \cdot 10^{-6}$	$2.63 \cdot 10^{-3}$
12		20	595±30	Fine	$1.70 \cdot 10^{-3}$	$4.60 \cdot 10^{-5}$	$5.34 \cdot 10^{-6}$	$8.95 \cdot 10^{-4}$
13		20	530±30	Fine	$1.64 \cdot 10^{-3}$	$5.50 \cdot 10^{-5}$	$5.56 \cdot 10^{-6}$	$9.87 \cdot 10^{-4}$
14		20	380±20	Fine	$1.60 \cdot 10^{-3}$	$5.80 \cdot 10^{-5}$	$4.23 \cdot 10^{-6}$	$7.27 \cdot 10^{-4}$
15	GO ₂	50	417±15	Coarse	$9.50 \cdot 10^{-4}$	$5.64 \cdot 10^{-5}$	$9.88 \cdot 10^{-6}$	$3.73 \cdot 10^{-4}$
16		50	388±20	Medium	$1.30 \cdot 10^{-3}$	$6.33 \cdot 10^{-5}$	$8.20 \cdot 10^{-6}$	$6.82 \cdot 10^{-4}$
17		50	380±8	Fine	$2.61 \cdot 10^{-3}$	$1.02 \cdot 10^{-5}$	$1.38 \cdot 10^{-5}$	$1.40 \cdot 10^{-3}$
18		20	362±21	Coarse	$1.60 \cdot 10^{-3}$	$5.09 \cdot 10^{-5}$	$5.79 \cdot 10^{-6}$	-
19		20	393±14	Medium	$8.64 \cdot 10^{-4}$	$3.41 \cdot 10^{-5}$	$4.48 \cdot 10^{-6}$	-
20		20	370±16	Fine	$2.75 \cdot 10^{-3}$	$2.45 \cdot 10^{-5}$	$1.12 \cdot 10^{-5}$	-
21		15	448±54	Fine	$2.70 \cdot 10^{-3}$	$1.80 \cdot 10^{-5}$	$1.07 \cdot 10^{-5}$	-
22		10	409±44	Fine	$4.25 \cdot 10^{-3}$	$1.34 \cdot 10^{-5}$	$8.98 \cdot 10^{-6}$	-
23	GO ₃	50	687±24	Coarse	$7.76 \cdot 10^{-4}$	$1.13 \cdot 10^{-4}$	$8.41 \cdot 10^{-6}$	$5.43 \cdot 10^{-5}$
24		50	679±19	Medium	$1.10 \cdot 10^{-3}$	$8.22 \cdot 10^{-5}$	$8.15 \cdot 10^{-6}$	$9.82 \cdot 10^{-4}$
25		50	727±28	Fine	$2.10 \cdot 10^{-3}$	$4.60 \cdot 10^{-5}$	$8.04 \cdot 10^{-6}$	$1.90 \cdot 10^{-3}$
26		20	650±15	Coarse	$1.10 \cdot 10^{-3}$	$4.03 \cdot 10^{-5}$	$4.83 \cdot 10^{-6}$	$1.50 \cdot 10^{-3}$
27		20	677±21	Medium	$1.80 \cdot 10^{-3}$	$3.51 \cdot 10^{-5}$	$7.03 \cdot 10^{-6}$	$1.40 \cdot 10^{-3}$
28		20	733±43	Fine	$1.90 \cdot 10^{-3}$	$4.04 \cdot 10^{-5}$	$4.37 \cdot 10^{-6}$	$3.70 \cdot 10^{-3}$
29		15	645±27	Fine	$3.60 \cdot 10^{-3}$	$5.47 \cdot 10^{-6}$	$3.46 \cdot 10^{-6}$	$8.90 \cdot 10^{-3}$
30		10	588±28	Fine	$4.60 \cdot 10^{-3}$	$1.02 \cdot 10^{-5}$	$5.45 \cdot 10^{-6}$	$8.40 \cdot 10^{-3}$
31		20	1167±111	Fine	$2.80 \cdot 10^{-3}$	$2.74 \cdot 10^{-5}$	$6.24 \cdot 10^{-6}$	$8.60 \cdot 10^{-3}$
32		20	868±41	Fine	$2.00 \cdot 10^{-3}$	$3.44 \cdot 10^{-5}$	$5.65 \cdot 10^{-6}$	$3.30 \cdot 10^{-3}$
33		20	450±15	Fine	$1.49 \cdot 10^{-3}$	$4.82 \cdot 10^{-5}$	$5.21 \cdot 10^{-6}$	$1.09 \cdot 10^{-3}$
34		20	270±60	Fine	$1.30 \cdot 10^{-3}$	$6.33 \cdot 10^{-5}$	$4.36 \cdot 10^{-6}$	$8.71 \cdot 10^{-4}$

323

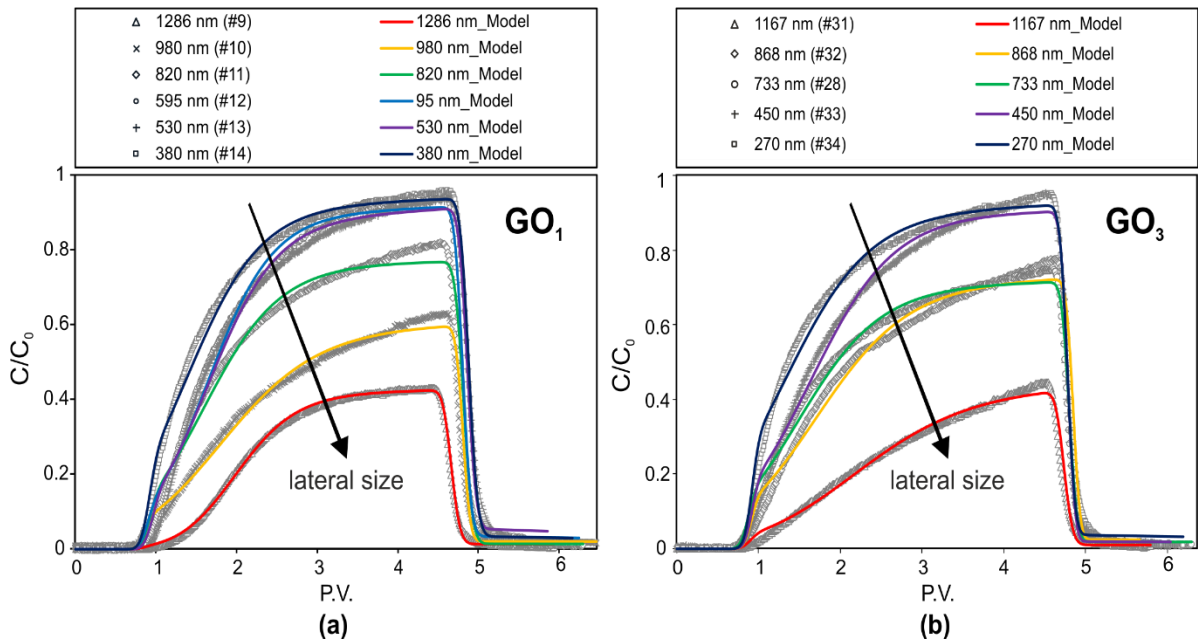
324

325 **3.2.1. Effect of lateral size and type of GONP**

326 For a given GO type, the average lateral size was adjusted by tuning the duration of the probe
327 sonication prior injection, following Figure S8. Figure 1 and Figure 2 report the experimental
328 and simulated BTCs and the measured retention profiles in columns packed with fine sand
329 (S₃) for different lateral sizes of GO₁ (tests no. 6 and 9-14) and GO₃ (test no. 28, 31-34) in the
330 range 300 to 1300 nm. The results revealed that the GO size strongly affects retention and
331 transport in saturated sand columns. The mobility of GONP tends to increase with decreasing
332 particle size. Mass balances (Table S1) indicate that the percentage of retained particles
333 decreases with decreasing the GO size, consistently with results reported by previous studies
334 for other types of particles, e.g. the work of Hu et al. (2017) for spherical carbon nanoparticles.
335 Thus, it suggests that particle shape, for our GONP, has no major influence in this sense.
336 However, a better insight into retention mechanisms is necessary.

337 Figure 2a shows that larger GO₁ produces strongly declining retention profiles, while smaller
338 GO₁ produces a more uniform distribution along the column. Previous studies mainly
339 observed GONP retention to be dominated by physical-chemical interactions with the porous
340 matrix, resulting in blocking phenomena (Dong et al., 2019; Dong et al., 2016; Dong et al.,
341 2017; Feriencikova and Xu, 2012; Liu et al., 2013b; Sun et al., 2015; Wang et al., 2018; Xia
342 et al., 2019). In our study we observed the same behavior for small particles, while for the
343 largest ones (close to or exceeding 1 micron) the declining retention profiles suggest that
344 physical retention also plays an important role. Particle size analysis on retained particles
345 (Figure S11) showed that, for these tests, larger particles are retained close to the column inlet,
346 and smaller ones travel longer distances; conversely, an almost constant size distribution was
347 observed when particles significantly smaller than 1 micron were injected.

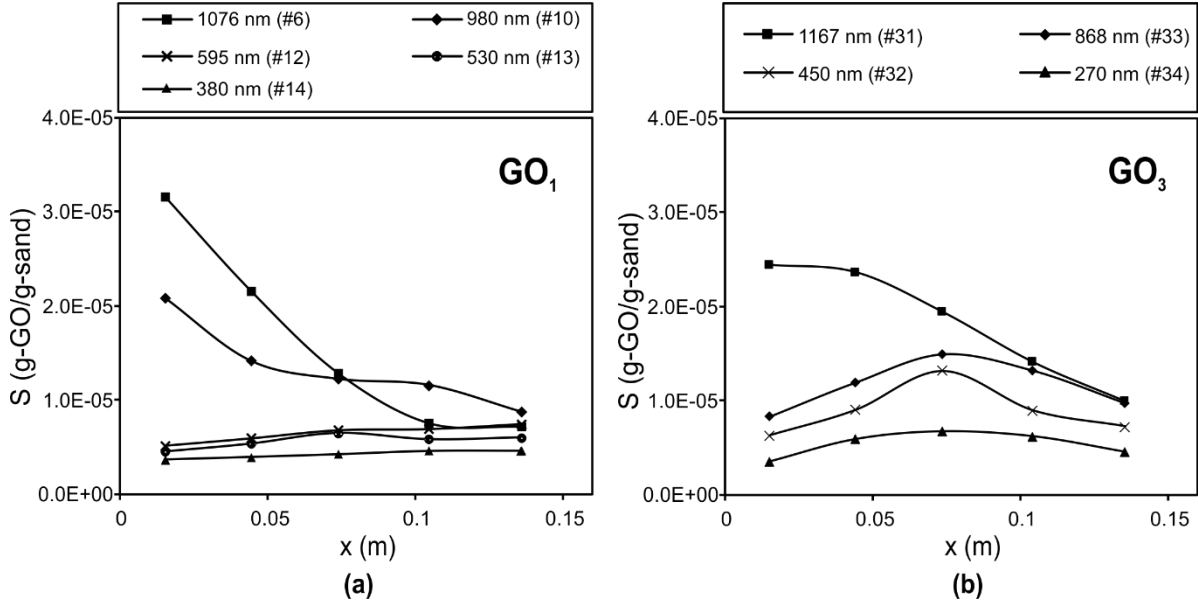
348



349

350 *Figure 1: Observed and simulated breakthrough curves (BTCs) of (a) GO_1 and (b) GO_3 with*
 351 *different lateral sizes at the same input concentrations of 20 mg/L in Sand S_3 . Symbols:*
 352 *experimental data/ Lines: simulation results*

353



354

355 *Figure 2: Observed retention profiles of (a) GO_1 and (b) GO_3 with different lateral sizes at*
 356 *the same input concentrations of 20 mg/L in Sand S_3*

357

358 Likely, the discussed behavior can be attributed to straining. This result is consistent with a
 359 previous study (Qi et al., 2014a) where the significant straining effect was reported for

360 heterogeneous (natural) saturated porous media. For rounded-shape colloids, it is commonly
361 accepted that straining is a relevant process if the ratio of particle (d_p) to finer sand size (d_{10})
362 $d_p/d_{10} > 0.008$ (Xu et al., 2006). For our sand S₃ (having $d_{10} = 75 \mu\text{m}$) this corresponds to
363 GONP of approximately 600 nm. As an evidence, clearly declining profiles were observed
364 for particles of 1 μm or larger, corresponding to a ratio $d_p/d_{10} \geq 0.013$.

365 For GO₃ (Figure 2b) a quite uncommon trend was obtained, with higher retention in the central
366 portion of the column. This is particularly evident for particles with intermediate size,
367 probably due to the relatively broad size distribution of these samples (Figure S8 II-b). Similar
368 non-monotonic trends have been recently attributed to competing deposition of non-
369 monodispersed colloids in fractures (Malgaresi et al., 2019). This trend was less evident for
370 the smallest particles (270 nm) with a fairly sharp particle size distribution, which tended to
371 produce more uniform retention profiles. For the largest ones (1167 nm) instead, a strongly
372 declining trend was observed due to the predominant effect of straining which masked the
373 competition effect.

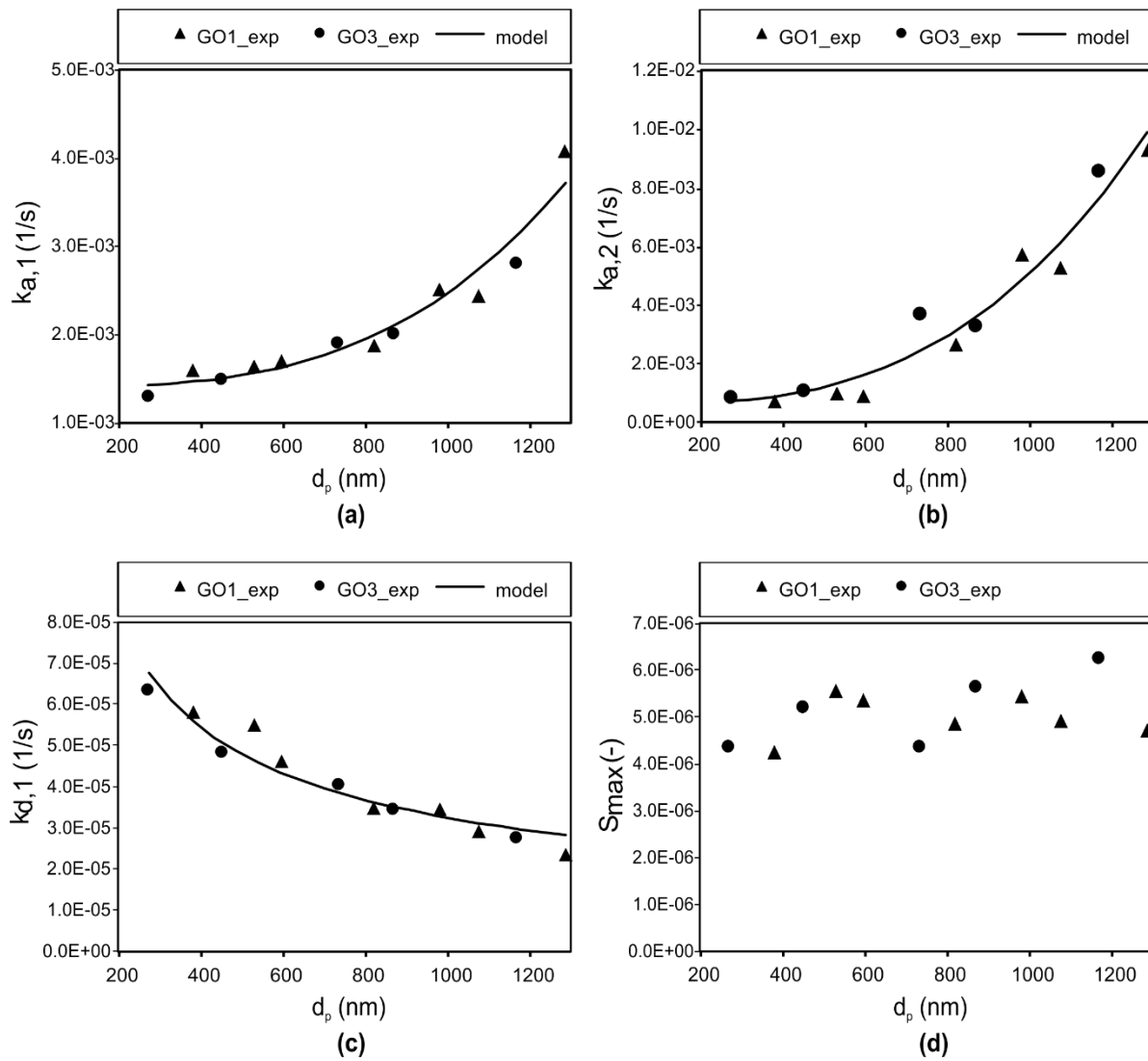
374 The fitted values of the model parameters (namely, $k_{a,1}$, $S_{\text{max},1}$, $k_{d,1}$, $k_{a,2}$) are reported in Table
375 2 and Figure 3. Fitted values of $S_{\text{max},1}$ oscillate in the range of $3.5\text{-}6.0 \cdot 10^{-6} \text{ g/g}$ (Figure 3b),
376 without any evident correlation between $S_{\text{max},1}$ and GO lateral size (d_p). This range is
377 comparable with the retained concentrations (S) measured for small particles (Figure 2) when
378 straining does not play a significant role. The attachment kinetics $k_{a,1}$ and $k_{a,2}$ both increase
379 with increasing particle size d_p (Figure 3a and c). Increasing $k_{a,1}$ with d_p means that smaller
380 GONP attach to the retention site 1 more slowly than larger ones, even if they all tend to reach
381 a similar saturation concentration. This is also reflected by the different steepness of
382 breakthrough curves for small particles in Figure 1.

383 Similar to $k_{a,1}$, the parameter $k_{a,2}$ increases with increasing d_p . For small particles, $k_{a,1}$ and $k_{a,2}$
384 are similar. Conversely, when straining becomes relevant, $k_{a,2}$ significantly exceeds $k_{a,1}$ and
385 retention due to blocking becomes negligible compared to straining. In this case, retention
386 profiles are strongly declining along the column and breakthrough curves tend to a plateau
387 concentration C/C_0 lower than 1, which represents an irreversible straining.

388 An empirical power function can be used to model the correlation of the three parameters
389 ($k_{a,1}$, $k_{d,1}$ and $k_{a,2}$) with d_p :

$$k_i = a + b d_p^c \quad (4)$$

390 where k_i is the generic attachment/detachment kinetic coefficient, and a , b , and c are fitting
391 parameters. For $k_{a,1}$ the fitted values are $a = 1.41 \cdot 10^{-3} \text{ s}^{-1}$, $b = 3.10 \cdot 10^{15} (\text{s} \cdot \text{m})^{-1}$, $c = 3.077$ with
392 $R^2 = 0.938$; for $k_{a,2}$ $a = 6.14 \cdot 10^{-4} \text{ s}^{-1}$, $b = 1.20 \cdot 10^{15} (\text{s} \cdot \text{m})^{-1}$, $c = 2.905$ with $R^2 = 0.947$; for $k_{d,1}$
393 $a = 4.37 \cdot 10^{-7} \text{ s}^{-1}$, $b = 1.28 \cdot 10^{-8} (\text{s} \cdot \text{m})^{-1}$, $c = -0.567$ with $R^2 = 0.915$. The fitted curves are
394 reported in Figure 3a-c as solid lines. The fitting is satisfactory for all coefficients, with R^2
395 values above 0.93 in all three cases. It is worth to notice that for all kinetic coefficients the
396 value represents the lowest, asymptotic kinetics for small (in case of attachment) or large (in
397 case of detachment) particles. A very similar exponent, close to 3, is found for $k_{a,1}$ and $k_{a,2}$.
398 The exponent for $k_{d,1}$ is negative reflecting the declining trend of the detachment kinetics with
399 increasing particle size.



400

401 *Figure 3: GONP deposition and release coefficients as a function of average particle size*
 402 *for GO1 and GO3: (a) $k_{a,1}$ (b) $k_{a,2}$ (c) $k_{d,1}$ and (d) S_{max}*

403

404 Interestingly, the results were very close to previous findings obtained for rounded-shaped
 405 colloids. The obtained trends of $k_{a,2}$ versus d_p are consistent with Bradford et al. (2003) who
 406 reported that a power function can represent a good correlation between $k_{a,2}$ and particle size
 407 for latex microparticles. Moreover, the exponent obtained from the detachment kinetic
 408 coefficient (-0.567) is very close to the theoretical value of -0.58 proposed by Rittman (1982)
 409 and later adopted by Brovelli et al. (2009) for the detachment of biofilms. However, further

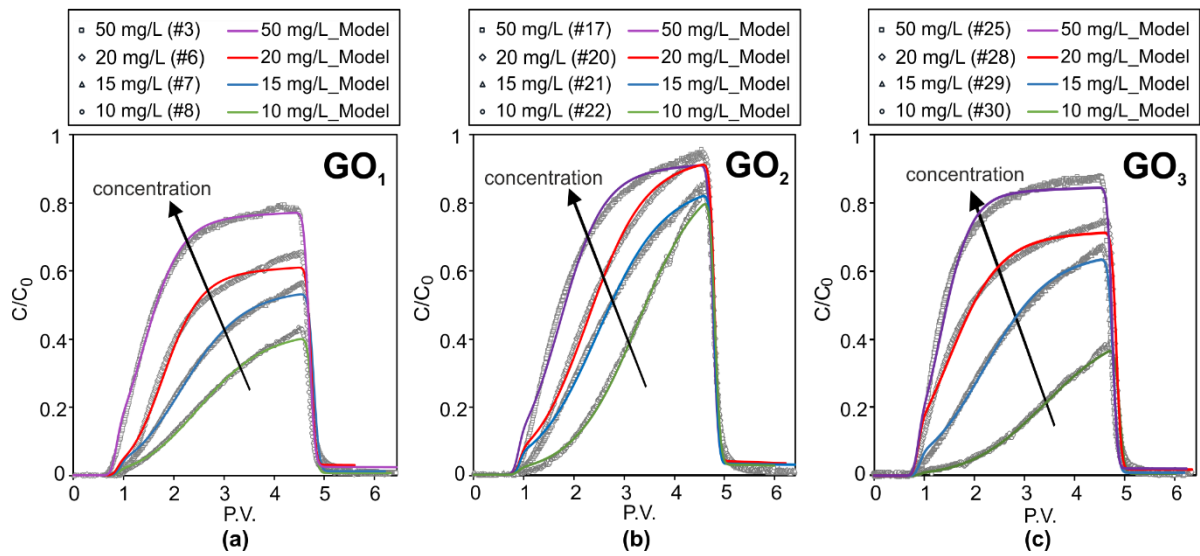
410 studies would be needed to understand if the empirical law of equation 4, or similar power
411 functions, can be generalized to any type of particles.

412 **3.2.2. Effect of input concentration**

413 The transport tests at different input mass concentration (C_0) were performed in columns
414 packed with sand S_3 (tests no. 3 and 6-8 for GO_1 , n. 17 and 20-22 for GO_2 , n. 25 and 28-30
415 for GO_3 , see Table 2). The GONP size is constant for each test performed with the same GO
416 type but different sizes were selected for GO_1 , GO_2 , and GO_3 , in order to have a set of tests
417 where, respectively, straining is relevant (for GO_1 , average size close to $1\ \mu\text{m}$), is not relevant
418 (GO_2 , approximately 400 nm) and is expected to play a role, but not to dominate transport
419 (GO_3 , 700 nm).

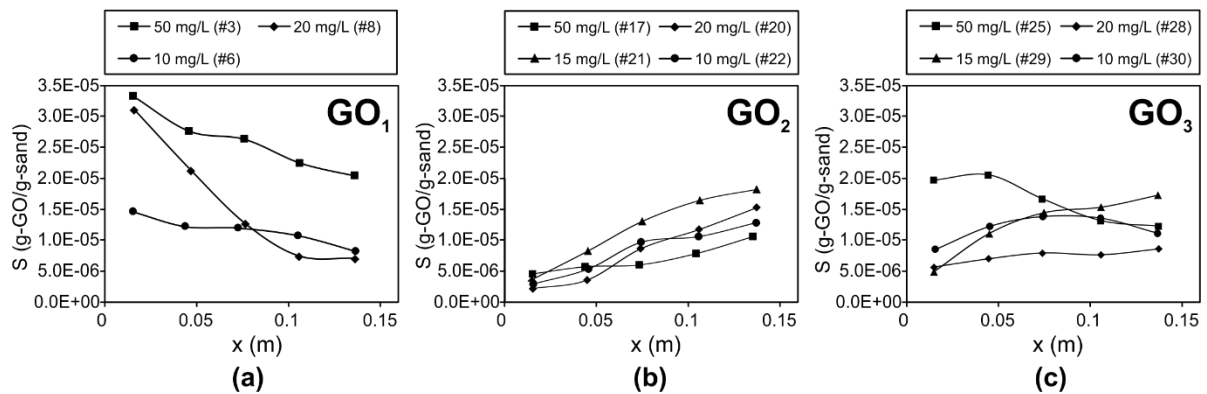
420 The breakthrough curves (Figure 4) show similar trends for all three types of GONP: changing
421 the input concentration in the range of 10 to 50 mg/L affected the transport and retention of
422 the nanoparticles. The mobility of all types of GO tends to increase with increasing the
423 injected concentration C_0 . This finding is consistent with Sun et al. (2015), the only previous
424 study, to our knowledge, investigating the influence of inlet concentration on the transport
425 and retention of GONP. Mass balance and mass recovery calculations (Table S1) confirm that
426 the total retained mass decreases with increasing C_0 . The observed behavior is coherent with
427 blocking-dominated deposition. In other words, a higher C_0 saturates the deposition sites more
428 rapidly compared with lower C_0 , thus increasing the overall mobility of the injected
429 suspension. Our tests with higher C_0 show a steeper increase of the breakthrough curves, even
430 if the effect is less pronounced for GO_2 , which is the sample with the overall highest mobility
431 and smallest particle size. It is noteworthy that some differences exist among the GO types.
432 However, based on the results discussed in the previous paragraph, it can be assumed that

433 these differences are related mainly to the different size of the three samples, rather than to
 434 possible minor differences in composition and surface properties.



435
 436 *Figure 4: Observed and simulated breakthrough curves (BTCs) of (a)GO₁ (Z-Ave. 1050±100 nm), (b)*
 437 *GO₂ (Z-Ave. 410±50 nm), and (c) GO₃ (Z-Ave. 650±100 nm) at different input concentrations from*
 438 *50 mg/L to 10 mg/L in sand S₃. Symbols: experimental data/ Lines: simulation results*

439



440
 441 *Figure 5: Observed retention profiles of (a) GO₁, (b) GO₂, and (c) GO₃ at different input*
 442 *concentrations from 50 mg/L to 10 mg/L in sand S₃.*

443

444 Considering the modeling of GONP transport, the fitting obtained is satisfactory for all
 445 breakthrough curves. For GO₁ and GO₃, the two-site deposition model correctly describes the
 446 GO transport. Conversely, for GO₂, characterized by the smallest particle size, straining is

447 irrelevant for all tests except those where the highest concentration (50 mg/L) is injected. This
448 suggests that, in such conditions, a stronger interaction arises between deposited particles and
449 those suspended in the pore water, promoting enhanced deposition processes.

450 The attachment and detachment kinetic coefficients $k_{a,1}$ and $k_{d,1}$ do not significantly change
451 with changing injected concentration. Conversely, a slight increase of $S_{\max,1}$ with increasing
452 injected concentration is observed, even if the explanation for this is unclear, and further
453 investigation would be needed to elucidate this aspect.

454

455 **3.2.3. Effect of sand grain size**

456 Figure 6 depicts the experimental and simulated BTCs of GO_1 (tests n. 1-6 in Table 2) injected
457 at 20 and 50 mg/L in sands S_1 (coarse), S_2 (medium) and S_3 (fine). The corresponding
458 retention profiles are reported in Figure 7. Also, for this set of tests, the size of the three GO
459 samples was adjusted to approximately 1 μm for GO_1 , 400 nm for GO_2 and 700 nm for GO_3 .

460 The results indicate that the sand grain size significantly affects the transport and retention of
461 GONP. The same tests performed using GO_2 (tests 15-20 in Table 2) and GO_3 (tests 23-28 in
462 Table 2) are reported in the Supporting Information (Figure S13) and show similar results.
463 The impact of sand size on the transport of GO_2 and GO_3 showed similar results.

464 As a general outcome, the mobility of GONP at a given C_0 tends to increase with increasing
465 the sand grain size. The highest breakthrough concentration is found in coarse sand. The
466 corresponding retention profile is almost constant along the column, thus indicating that
467 straining is limited or even negligible. Conversely, reducing the grain size, the breakthrough
468 decreases, and straining becomes more relevant. The mass balances (Table 1) confirm that

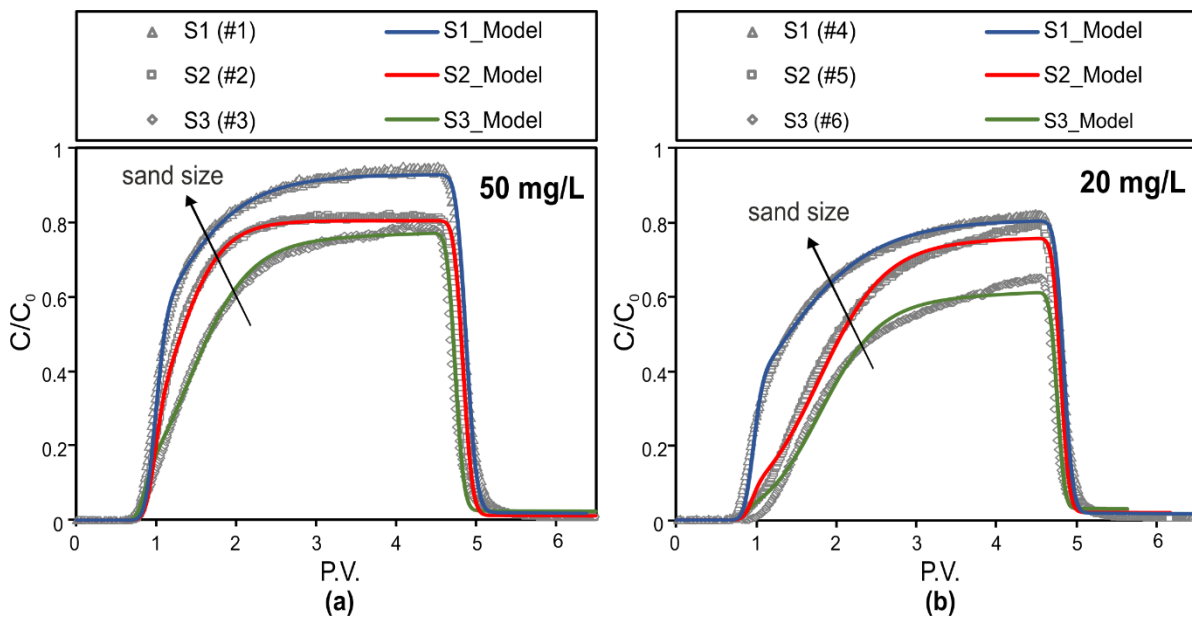
469 decreasing the sand size lead the total retention to significantly increase for all GO types and
470 both injected concentrations.

471 The fitted parameters reported in Table 2 indicate how changing the sand size affects the
472 relative importance of blocking and straining retention mechanisms. As for physical-chemical
473 deposition following the blocking dynamics, the attachment kinetic coefficient $k_{a,1}$ increases
474 with decreasing sand size (from S_1 to S_3), and coherently $k_{d,1}$ decreases for both injected
475 concentrations. This was expected from the established literature on colloid removal
476 efficiency in granular media (Messina et al., 2016; Sun et al., 2015; Tufenkji and Elimelech,
477 2004; Yao et al., 1971). Some other experimental studies investigating the effect of the grain
478 size on the particle attachment rate (Bradford and Bettahar, 2006; Kasel et al., 2012; Liang et
479 al., 2013; Sun et al., 2015; Torkzaban et al., 2010) achieved the similar results, even if the
480 great majority of such studies focused on spherical colloidal particles, e.g. carboxyl latex,
481 QDs, and AgNPs.

482 Differences in the maximum retainable concentration due to physico-chemical interactions
483 ($S_{max,1}$) among the three sand samples are attributable to differences in SSA, since no
484 significant difference in zeta potential was observed. As a general rule, the fitted values of
485 $S_{max,1}$ (Table 2) increase with decreasing sand size (i.e. from S_1 to S_3) for a given GO type and
486 injected concentration; this results in $S_{max,1}$ values for S_3 approximately two times higher than
487 the $S_{max,1}$ obtained for S_1 , in agreement with SSA of sand grains (assuming spherical grains,
488 SSA for S_1 and S_3 is respectively 0.008 and 0.003 m²/kg, being the average grain size 0.75
489 and 0.28 mm).

490 Straining also contributed to the retention of GONP and affected the shape of profiles of
491 retained particles. Based on the considerations discussed in the previous paragraphs, straining
492 is expected to occur for GO_1 and, limitedly, for GO_2 . Back again to the ratio d_p/d_{10} and the

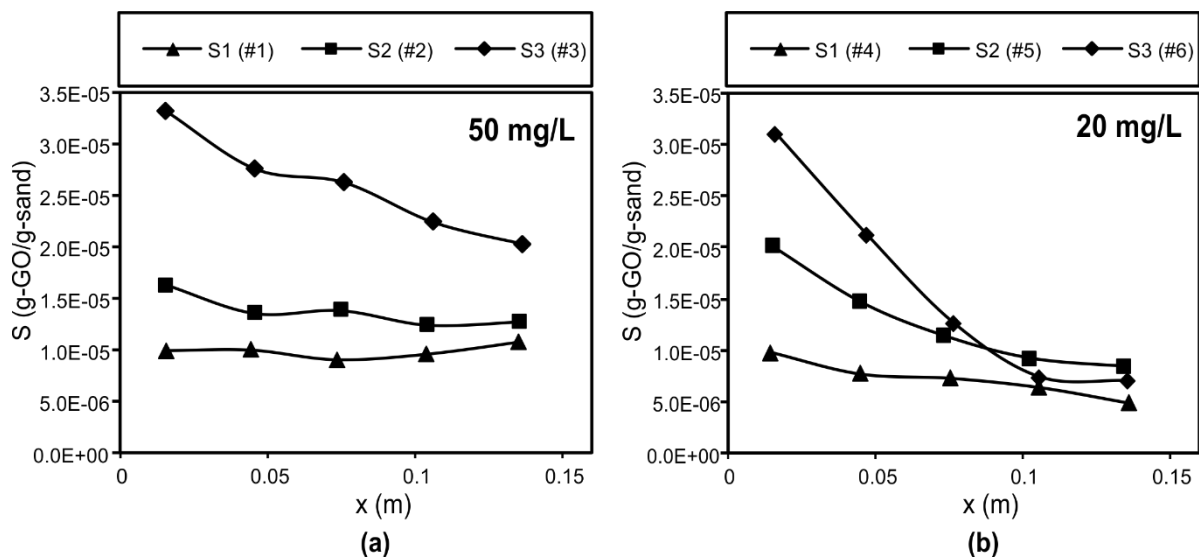
493 straining limit of 0.008 (Xu et al., 2006), GO_1 was expected to exceed this threshold value in
 494 sand S_3 , and to approach the limit for S_2 . Coherently, the retention profiles (Figure 7) showed
 495 a steep decrease for S_3 and a less pronounced decrease for S_2 . The fitted straining coefficients
 496 $k_{a,2}$ are lower for coarse sand and increase with decreasing sand size. Changes in $k_{a,2}$ from S_1
 497 to S_3 cover approximately one order of magnitude (typically from 10^{-4} s^{-1} to 10^{-3} s^{-1}) and are
 498 more evident at the highest injected concentration (for example, compare the values of $k_{a,2}$ for
 499 GO_1 and GO_3 injected at 50 mg/L).



500

501 *Figure 6: Observed and simulated breakthrough curves for GO_1 , injected in columns*
 502 *packed with sand S_1 , S_2 , and S_3 at a concentration of 50 mg/L and 20 mg/L.*

503



504

505 *Figure 7: Observed retention profiles of GO₁ with two different input concentrations of (a)*
 506 *50 mg/L and (b) 20 mg/L in various sand sizes of S₁ (coarse), S₂ (medium), and S₃ (fine).*

507

508 **4. Conclusions**

509 This study showed that GONP can be stably dispersed in water and are remarkably mobile
 510 when injected in silica sand. The experimental results also showed that a parameter having a
 511 major impact on GONP mobility is the particle lateral size; also the size ratio of particle to
 512 sand grains is relevant. Conversely, the source of graphene oxide (i.e. synthesized in the
 513 laboratory or provided by commercial producers) had a minor impact, even if the C and O
 514 content of the three GONP types was not identical. This suggests that the outcomes of this
 515 study could potentially be extended also to other GONP not considered here. The injected
 516 concentration affected the mobility of the particles but, at least in the range herein explored,
 517 has had no dramatic effect.

518 Despite the peculiar shape of GONP compared to more conventional colloids, the advection-
 519 dispersion-deposition equation commonly used for colloid transport in porous media was still
 520 adequate to describe the transport of these particles. The experimental and modeling results
 521 indicated that both physico-chemical (blocking) and physical (straining) retention

522 mechanisms strongly influence the transport and retention of GONP. Blocking is observed in
523 all cases and is coherent with the good colloidal stability of the particles. Straining becomes
524 relevant for larger particles and/or finer sand, as expected from round-shaped colloids, and
525 plays a relevant role only for particles exceeding approximately 0.5-1% of the sand d_{10} .
526 Therefore, the retention associated to the physical interaction of GONP with the porous
527 medium cannot be neglected.

528 Concerning the potential application to groundwater remediation, the results of this study are
529 very promising. GONP are sufficiently mobile to expect a relatively easy injection in the field,
530 and the possibility to control their migration and deposition in the subsoil by modifying the
531 particle size.

532

533 **5. Acknowledgments**

534 Authors would like to acknowledge prof. Matteo Pavese (DISAT – Politecnico di Torino) and
535 his group for the support in graphene oxide synthesis, and the personnel of laboratories at
536 DIATI - Politecnico di Torino and of the Department of Civil and Environment, Polytechnic
537 University of Tehran (Amirkabir) for their appreciated help with experiments and chemical
538 analyses. The work was conducted in the laboratories of Politecnico di Torino and was partly
539 supported by Iran National Science Foundation (INSF) [grant number 95815221] and Iran
540 Nanotechnology Initiative Council (INIC) [grant number 107029].

541

542 **6. Competing interests statement**

543 The authors have no competing interests

544

545

- 547 Akpotu SO, Moodley B. Application of as-synthesised MCM-41 and MCM-41 wrapped with reduced graphene
548 oxide/graphene oxide in the remediation of acetaminophen and aspirin from aqueous system. *Journal of*
549 *Environmental Management* 2018; 209: 205-215.
- 550 Bianco C, Tosco T, Sethi R. A 3-dimensional micro- and nanoparticle transport and filtration model (MNM3D) applied to
551 the migration of carbon-based nanomaterials in porous media. *Journal of Contaminant Hydrology* 2016; 193: 10-
552 20.
- 553 Bradford SA, Bettahar M. Concentration dependent transport of colloids in saturated porous media. 2006; 82: 99-117.
- 554 Bradford SA, Bettahar M, Simunek J, van Genuchten MT. Straining and Attachment of Colloids in Physically Heterogeneous
555 Porous Media. *Vadose Zone Journal* 2004; 3: 384-394.
- 556 Bradford SA, Kim HN, Haznedaroglu BZ, Torkzaban S, Walker SL. Coupled Factors Influencing Concentration-Dependent
557 Colloid Transport and Retention in Saturated Porous Media. 2009; 43: 6996-7002.
- 558 Bradford SA, Simunek J, Bettahar M, Van Genuchten MT, Yates SR. Modeling Colloid Attachment, Straining, and
559 Exclusion in Saturated Porous Media. 2003.
- 560 Brovelli A, Malaguerra F, Barry DA. Bioclogging in porous media: Model development and sensitivity to initial conditions.
561 *Environmental Modelling & Software* 2009; 24: 611-626.
- 562 Camesano TA, Logan BE. Influence of Fluid Velocity and Cell Concentration on the Transport of Motile and Nonmotile
563 Bacteria in Porous Media. 1998: 1699-1708.
- 564 Chen D, Feng H, Li J. Graphene oxide: preparation, functionalization, and electrochemical applications. *Chem Rev* 2012;
565 112: 6027-53.
- 566 Chen J, Yao B, Li C, Shi G. An improved Hummers method for eco-friendly synthesis of graphene oxide. *Carbon* 2013; 64:
567 225-229.
- 568 Chrysikopoulos CV, Sotirelis NP, Kallithrakas-Kontos NG. Cotransport of Graphene Oxide Nanoparticles and Kaolinite
569 Colloids in Porous Media. *Transport in Porous Media* 2017; 119: 181-204.
- 570 Corsi I, Winther-nielsen M, Sethi R, Punta C, Torre CD, Libralato G, et al. Ecofriendly nanotechnologies and nanomaterials
571 for environmental applications : Key issue and consensus recommendations for sustainable and ecosafe
572 nanoremediation. *Ecotoxicology and Environmental Safety* 2018; 154: 237-244.
- 573 Dong S, Gao B, Sun Y, Guo H, Wu J, Cao S, et al. Visualization of graphene oxide transport in two-dimensional
574 homogeneous and heterogeneous porous media. *Journal of Hazardous Materials* 2019; 369: 334-341.
- 575 Dong S, Shi X, Gao B, Wu J, Sun Y, Guo H, et al. Retention and Release of Graphene Oxide in Structured Heterogeneous
576 Porous Media under Saturated and Unsaturated Conditions. *Environmental Science & Technology* 2016; 50:
577 10397-10405.
- 578 Dong S, Sun Y, Gao B, Shi X, Xu H, Wu J, et al. Retention and transport of graphene oxide in water-saturated limestone
579 media. *Chemosphere* 2017; 180: 506-512.
- 580 Fan W, Jiang X, Lu Y, Huo M, Lin S, Geng Z. Effects of surfactants on graphene oxide nanoparticles transport in saturated
581 porous media. *Journal of Environmental Sciences (China)* 2015a; 35: 12-19.
- 582 Fan W, Jiang XH, Yang W, Geng Z, Huo MX, Liu ZM, et al. Transport of graphene oxide in saturated porous media: Effect
583 of cation composition in mixed Na–Ca electrolyte systems. *Science of The Total Environment* 2015b; 511: 509-
584 515.
- 585 Feriencikova L, Xu S. Deposition and remobilization of graphene oxide within saturated sand packs. *Journal of Hazardous*
586 *Materials* 2012; 235-236: 194-200.
- 587 Godinez IG, Darnault CJG. Aggregation and transport of nano-TiO₂ in saturated porous media: Effects of pH, surfactants
588 and flow velocity. *Water Research* 2011; 45: 839-851.
- 589 Hosseini SM, Tosco T. Transport and retention of high concentrated nano-Fe/Cu particles through highly flow-rated packed
590 sand column. *Water Research* 2013; 47: 326-338.
- 591 Hu Z, Zhao J, Gao H, Nourafkan E, Wen D, Hu Z, et al. Transport and Deposition of Carbon Nanoparticles in Saturated
592 Porous Media. *Energies* 2017; 10: 1151.
- 593 Huang X, Yin Z, Wu S, Qi X, He Q, Zhang Q, et al. Graphene-based materials: Synthesis, characterization, properties, and
594 applications. *Small* 2011; 7: 1876-1902.
- 595 Iqbal MZ, Abdala AA. Oil spill cleanup using graphene. 2013: 3271-3279.
- 596 Jian-Zhou H, Cheng-Cheng L, Deng-Jun W, Zhou D-M. Biofilms and extracellular polymeric substances mediate the
597 transport of graphene oxide nanoparticles in saturated porous media. *Journal of Hazardous Materials* 2015; 300:
598 467-474.
- 599 Jiang Y, Zhang X, Yin X, Sun H, Wang N. Graphene oxide-facilitated transport of Pb²⁺ and Cd²⁺ in saturated porous media.
600 *Science of the Total Environment* 2018; 631-632: 369-376.
- 601 Johnson PR, Sun N, Elimelech M. Colloid transport in physically and geochemically heterogeneous porous media_
602 Modeling, measurements, and parameter identification.pdf. *Environmental Science and Technology* 1996; 30:
603 3284-3293.
- 604 Karn B, Kuiken T, Otto M. Nanotechnology and in Situ Remediation : A Review of the Benefits and. 2009; 117: 1823-1831.
- 605 Kasel D, Bradford SA, Klumpp E, Gru P. Transport and retention of multi-walled carbon nanotubes in saturated porous
606 media : Effects of input concentration and grain size. 2012; 7.
- 607 Lanphere JD, Luth CJ, Walker SL. Effects of Solution Chemistry on the Transport of Graphene Oxide in Saturated Porous
608 Media. *Environmental Science & Technology* 2013; 47: 4255-4261.

609 Lanphere JD, Rogers B, Luth C, Bolster CH, Walker SL. Stability and Transport of Graphene Oxide Nanoparticles in
610 Groundwater and Surface Water. *Environ Eng Sci* 2014; 31: 350-359.

611 Li Y, Yang N, Du T, Wang X, Chen W. Transformation of graphene oxide by chlorination and chloramination: Implications
612 for environmental transport and fate. *Water Res* 2016; 103: 416-423.

613 Liang Y, Bradford SA, Simunek J, Vereecken H, Klumpp E. Sensitivity of the transport and retention of stabilized silver
614 nanoparticles to physicochemical factors. *Water Research* 2013; 47: 2572-2582.

615 Liu J, Cui L, Losic D. Graphene and graphene oxide as new nanocarriers for drug delivery applications. *Acta Biomaterialia*
616 2013a; 9: 9243-9257.

617 Liu L, Gao B, Wu L, Morales VL, Yang L, Zhou Z, et al. Deposition and transport of graphene oxide in saturated and
618 unsaturated porous media. *Chemical Engineering Journal* 2013b; 229: 444-449.

619 Liu L, Gao B, Wu L, Yang L, Zhou Z, Wang H. Effects of pH and surface metal oxyhydroxides on deposition and transport
620 of carboxyl-functionalized graphene in saturated porous media. *Journal of Nanoparticle Research* 2013c; 15.

621 Lotya M, Rakovich A, Donegan JF, Coleman JN. Measuring the lateral size of liquid-exfoliated nanosheets with dynamic
622 light scattering. *Nanotechnology* 2013; 24.

623 Lu T, Xia T, Qi Y, Chengdong Z, Chen W. Effect of clay materials on transport of graphene oxide in saturated porous media.
624 2017; 36: 655-660.

625 Malgaresi G, Collins B, Alvaro P, Bedrikovetsky P. Explaining non-monotonic retention profiles during flow of size-
626 distributed colloids. *Chemical Engineering Journal* 2019; 375: 121984.

627 Messina F, Tosco T, Sethi R. On the failure of upscaling the single-collector efficiency to the transport of colloids in an array
628 of collectors. *Water Resources Research* 2016; 52: 5492-5505.

629 Montes-Navajas P, Asenjo NG, Santamaría R, Menéndez R, Corma A, García H. Surface area measurement of graphene
630 oxide in aqueous solutions. *Langmuir* 2013; 29: 13443-13448.

631 Novoselov KS, Fal VI, Colombo L, Gellert PR, Schwab MG, Kim K. REVIEW A roadmap for graphene. *Nature* 2012; 490:
632 192-200.

633 O'Carroll D, Sleep B, Krol M, Boparai H, Kocur C. Nanoscale zero valent iron and bimetallic particles for contaminated site
634 remediation. *Advances in Water Resources* 2013; 51: 104-122.

635 Patil SS, Shedbalkar UU, Truskewycz A, Chopade BA, Ball AS. Environmental Technology & Innovation Nanoparticles for
636 environmental clean-up : A review of potential risks and emerging solutions. *Environmental Technology &*
637 *Innovation* 2016; 5: 10-21.

638 Paulchamy B, Arthi G, Lignesh B. A Simple Approach to Stepwise Synthesis of Graphene Oxide Nanomaterial. *Journal of*
639 *Nanomedicine & Nanotechnology* 2015; 06: 2-5.

640 Peng S, Wu D, Ge Z, Tong M, Kim H. Influence of graphene oxide on the transport and deposition behaviors of colloids in
641 saturated porous media. *Environmental Pollution* 2017; 225: 141-149.

642 Qi Z, Zhang L, Chen W. Transport of graphene oxide nanoparticles in saturated sandy soil. *Environmental Sciences:*
643 *Processes and Impacts* 2014a; 16: 2268-2277.

644 Qi Z, Zhang L, Wang F, Hou L, Chen W. Factors controlling transport of graphene oxide nanoparticles in saturated sand
645 column. 2014b; 33: 998-1004.

646 Rittman BE. The effect of shear stress on biofilm loss rate. *Biotechnology and Bioengineering* 1982; 24: 501-506.

647 Shahriary L, Athawale AA. Graphene Oxide Synthesized by using Modified Hummers Approach. *International Journal of*
648 *Renewable Energy and Environmental Engineering* 2014; 02: 58-63.

649 Sun L, Yu H, Fugetsu B. Graphene oxide adsorption enhanced by in situ reduction with sodium hydrosulfite to remove
650 acridine orange from aqueous solution. *Journal of Hazardous Materials* 2012; 203-204: 101-110.

651 Sun Y, Gao B, Bradford SA, Wu L, Chen H, Shi X, et al. Transport, retention, and size perturbation of graphene oxide in
652 saturated porous media: Effects of input concentration and grain size. *Water Research* 2015; 68: 24-33.

653 Torkzaban S, Kim Y, Mulvihill M, Wan J, Tokunaga TK. Transport and deposition of functionalized CdTe nanoparticles in
654 saturated porous media. *Journal of Contaminant Hydrology* 2010; 118: 208-217.

655 Tortello M, Colonna S, Bernal M, Gomez J, Pavese M, Novara C, et al. Effect of thermal annealing on the heat transfer
656 properties of reduced graphite oxide flakes: A nanoscale characterization via scanning thermal microscopy. *Carbon*
657 2016; 109: 390-401.

658 Tosco T, Bosch J, Meckenstock RU, Sethi R. Transport of ferrihydrite nanoparticles in saturated porous media: Role of ionic
659 strength and flow rate. *Environmental Science and Technology* 2012; 46: 4008-4015.

660 Tosco T, Petrangeli M, Cruz C, Sethi R. Nanoscale zerovalent iron particles for groundwater remediation : a review. *Journal*
661 *of Cleaner Production* 2014; 77: 10-21.

662 Tosco T, Sethi R. Transport of non-newtonian suspensions of highly concentrated micro- and nanoscale iron particles in
663 porous media: A modeling approach. *Environmental Science and Technology* 2010; 44: 9062-9068.

664 Tosco T, Tiraferri A, Sethi R. Ionic Strength Dependent Transport of Microparticles in Saturated Porous Media: Modeling
665 Mobilization and Immobilization Phenomena under Transient Chemical Conditions. *Environmental Science &*
666 *Technology* 2009; 43: 4425-4431.

667 Tufenkji N, Elimelech M. Correlation Equation for Predicting Single-Collector Efficiency in Physicochemical Filtration in
668 Saturated Porous Media. 2004; 38: 529-536.

669 Wang C, Bobba AD, Attinti R, Shen C, Lazouskaya V, Wang L-P, et al. Retention and Transport of Silica Nanoparticles in
670 Saturated Porous Media: Effect of Concentration and Particle Size. 2012.

671 Wang D, Paradelo M, Bradford SA, Peijnenburg WJGM, Chu L, Zhou D. Facilitated transport of Cu with hydroxyapatite
672 nanoparticles in saturated sand: Effects of solution ionic strength and composition. *Water Research* 2011; 45: 5905-
673 5915.

674 Wang M, Gao B, Tang D, Sun H, Yin X, Yu C. Effects of temperature on graphene oxide deposition and transport in saturated
675 porous media. *J Hazard Mater* 2017; 331: 28-35.

676 Wang M, Gao B, Tang D, Yu C. Concurrent aggregation and transport of graphene oxide in saturated porous media : Roles
677 of temperature , cation type , and electrolyte. *Environmental Pollution* 2018; 235: 350-357.

678 Xia T, Qi Y, Zhu L, Qi Z, Chen W. Transport and retention of reduced graphene oxide materials in saturated porous media
679 : Synergistic effects of enhanced attachment and particle aggregation *. 2019; 247: 383-391.

680 Xu S, Gao B, Saiers JE. Straining of colloidal particles in saturated porous media. *Water Resources Research* 2006; 42.

681 Yang X, Li J, Wen T, Ren X, Huang Y, Wang X. *Colloids and Surfaces A : Physicochemical and Engineering Aspects*
682 Adsorption of naphthalene and its derivatives on magnetic graphene composites and the mechanism investigation.
683 *Colloids and Surfaces A: Physicochemical and Engineering Aspects* 2013; 422: 118-125.

684 Yao K-M, Habibi MT, O'Melia CR. *Water and Waste Water Filtration: Concepts and Applications*. 1971; 5: 1105-1112.

685 Yin X, Jiang Y, Tan Y, Meng X, Sun H, Wang N. Co-transport of graphene oxide and heavy metal ions in surface-modified
686 porous media. *Chemosphere* 2019; 218: 1-13.

687 Zhang W, Morales VnL, Cakmak ME, Salvucci AE, Geohring LD, Hay AG, et al. Colloid Transport and Retention in
688 Unsaturated Porous Media: Effect of Colloid Input Concentration. *Environmental Science & Technology* 2010;
689 44: 4965-4972.

690 Zhao K, Chen C, Cheng T, Shang J. Graphene oxide-facilitated uranium transport and release in saturated medium : Effect
691 of ionic strength and medium structure. *Environmental Pollution* 2019; 247: 668-677.

692 Zhou DD, Jiang XH, Lu Y, Fan W, Huo MX, Crittenden JC. Cotransport of graphene oxide and Cu(II) through saturated
693 porous media. *Science of the Total Environment* 2016; 550: 717-726.

694